Complex dynamics of an archetypal self-excited SD oscillator driven by moving belt friction*

Zhi-Xin Li(李志新)[1], Qing-Jie Cao(曹庆杰)[1,†], and Léger Alain[2]

[1] School of Astronautics, Harbin Institute of Technology, Harbin 150001, China
[2] Laboratoire de Mécanique et d'Acoustique, CNRS, 31, Chemin Joseph Aiguier, 13402 Marseille Cedex 20, France

(Received 28 June 2015; revised manuscript received 6 August 2015; published online 30 November 2015)

We propose an archetypal self-excited system driven by moving belt friction, which is constructed with the smooth and discontinuous (SD) oscillator proposed by the Cao *et al*. and the classical moving belt. The moving belt friction is modeled as the Coulomb friction to formulate the mathematical model of the proposed self-excited SD oscillator. The equilibrium states of the unperturbed system are obtained to show the complex equilibrium bifurcations. Phase portraits are depicted to present the hyperbolic structure transition, the multiple stick regions, and the friction-induced asymmetry phenomena. The numerical simulations are carried out to demonstrate the friction-induced vibration of multiple stick-slip phenomena and the stick-slip chaos in the perturbed self-excited system. The results presented here provide an opportunity for us to get insight into the mechanism of the complex friction-induced nonlinear dynamics in mechanical engineering and geography.

Keywords: self-excited smooth and discontinuous (SD) oscillator, multiple stick regions, friction-induced asymmetry, stick-slip chaos

PACS: 05.45.–a, 05.45.Ac, 05.10.–a **DOI:** 10.1088/1674-1056/25/1/010502

1. Introduction

Much attention has been paid to the self-excited vibration induced by friction in practical mechanical engineering systems, i.e., brake,[1–3] chattering machine tools,[4,5] drill string,[6,7] and others. Most of the investigations in the literature are based on the conventional mass-on-moving-belt models to describe the friction-induced vibration in engineering systems. The majority of the works have been focused on the model which is characterized by a linear oscillator vibrating on the moving belt to derive the complex dynamics induced by friction, such as periodic motion,[8,9] chaotic behavior,[10] stick-slip vibration,[11,12] and Hopf-bifurcations.[13] However, even nonlinear friction dynamics has been of interest by introducing a cubic term into the harmonic oscillator on the moving belt in recent years,[14–16] few nonlinear phenomena induced by friction are explored in comparison with the conventional friction-induced periodic solution, chaos, and stick-slip vibrations. In fact, there are many nonlinear friction systems characterized by geometric nonlinearities of elastic large deformation or large displacement in mechanical engineering, for example, the geometric nonlinear vibration induced by friction between the brake disc and pad in a brake system,[17–19] the moving tectonic plates in an earthquake fault moving across each other,[20,21] and the ice stream and moving subglacial bed of Whillans Ice Stream (WIS) capable of stick-slip motion.[22]

At present, the research on the geometric nonlinear friction dynamics is very insufficient, and very few studies concerning the coupling from a theoretical point of view in the case of nonlinear friction and geometric nonlinearity exist. Therefore, it is necessary to construct a nonlinear friction system with geometric nonlinearity for getting insight into the mechanism of the complex friction-induced nonlinear dynamics in mechanical engineering and geography.

The motivation of this paper is to propose a novel friction system with geometric nonlinearity for truly revealing the dynamical characteristics of the geometric nonlinear friction systems in engineering and geography based on the well-known geometrical model[23] of SD oscillator proposed by Cao *et al.*[24–26] together with the classical moving belt, which is called the self-excited SD oscillator. Another motivation is to demonstrate multiple stick regions and the asymmetry induced by belt friction for this self-excited system. Furthermore, the complex dynamic behaviors of the perturbed self-excited SD oscillator are illustrated numerically to present the friction-induced vibration of multiple stick-slip phenomena and coexisting attractors. Through these investigations of self-excited SD oscillator, we gain a deeper understanding of geometric nonlinear friction dynamics in mechanical engineering and geography.

*Project supported by the National Natural Science Foundation of China (Grant Nos. 11372082 and 11572096) and the National Basic Research Program of China (Grant No. 2015CB057405).

†Corresponding author. E-mail: qingjiecao@hotmail.com

© 2016 Chinese Physical Society and IOP Publishing Ltd

2. The governing equation

The system analyzed in this paper is composed of a block of mass M, supported by a moving belt and connected to a fixed support by an inclined linear spring of stiffness coefficient K, which is capable of resisting both tension and compression, as shown in Fig. 1(a). The contact surface between the mass and the belt is rough, and the belt exerts a friction force on the mass. The mass vibrates under the influence of dry friction F_S modeled as Coulomb friction existing in the contact zone created by the mass's surface and the outer belt's surface. The belt moves with a constant velocity V_0. We assume a non-deformable moving belt, and the mass is secured to move in the horizontal direction without leaving the belt. The position of the mass over the belt is represented by X.

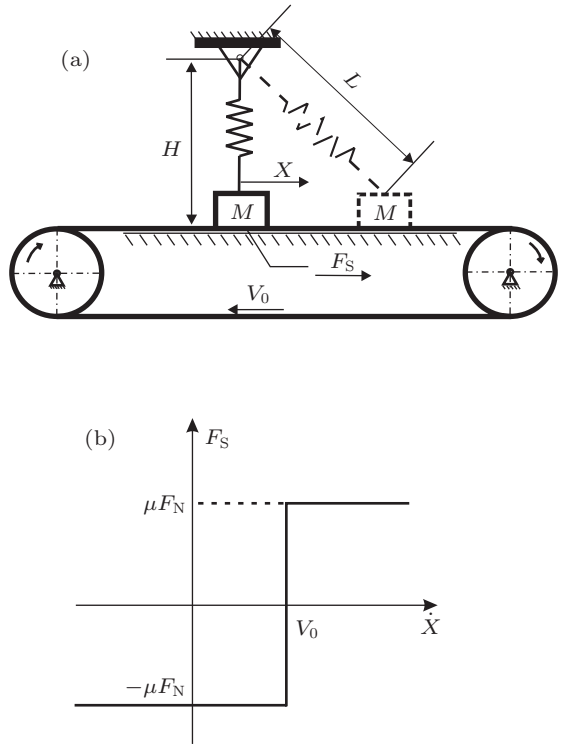


Fig. 1. (a) The dynamical model in the form of a self-excited oscillator, where a mass linked by an elastic spring vibrates on the moving belt. (b) Coulomb friction law.

The equation of motion for this mass–spring on the moving belt is given by

$$M\ddot{X}+KX\left(1-\frac{L}{\sqrt{X^2+H^2}}\right)+F_S=0, \tag{1}$$

where L is the original length of the spring, and H is the distance between the fixed point and the belt. The Coulomb friction force F_S between the mass and the belt is illustrated in Fig. 1(b), which can be described in the differential inclusion of Filippov type[27] as

$$F_S\in\mu F_N\mathrm{Sign}(\dot{X}-V_0), \tag{2}$$

where μ is the friction coefficient of contacting surfaces and assumed to be constant in this friction model, $F_N=Mg-KH(1-L/\sqrt{X^2+H^2})$ is the total force of the gravity of the mass and the vertical component of the spring force, $\dot{X}-V_0$ is the relative velocity of the mass and the belt, and

$$\mathrm{Sign}(\dot{X}-V_0)=\begin{cases}1, & \dot{X}>V_0,\\ [-1,1], & \dot{X}=V_0,\\ -1, & \dot{X}<V_0.\end{cases}$$

Equation (1) can be made dimensionless by letting $x=X/L$, $\omega_0^2=K/M$, $\alpha=H/L$, $g_1=g/(L\omega_0^2)$, $v_0=V_0/(L\omega_0)$, and $\tau=\omega_0 t$. Together with Eq. (2), it can be written as

$$\ddot{x}+x\left(1-\frac{1}{\sqrt{x^2+\alpha^2}}\right)\in-\mu\left[g_1-\alpha\left(1-\frac{1}{\sqrt{x^2+\alpha^2}}\right)\right]\mathrm{Sign}(\dot{x}-v_0), \tag{3}$$

where the dot denotes the derivative with respect to τ.

If system (1) is perturbed by a viscous damping of coefficient C and an external harmonic excitation of amplitude F and frequency Ω, the equation of motion can be written as

$$M\ddot{X}+C\dot{X}+KX\left(1-\frac{L}{\sqrt{X^2+H^2}}\right)\in F\cos\Omega t-\mu\left[Mg-KH\left(1-\frac{L}{\sqrt{X^2+H^2}}\right)\right]\mathrm{Sign}(\dot{X}-V_0). \tag{4}$$

The dimensionless equation of motion for this system is obtained by letting $x=X/L$, $c=C/(M\omega_0)$, $\omega_0^2=K/M$, $\alpha=H/L$, $g_1=g/(L\omega_0^2)$, $v_0=V_0/(L\omega_0)$, $f=F/(KL)$, $\omega=\Omega/\omega_0$, and $\tau=\omega_0 t$

$$\ddot{x}+c\dot{x}+x\left(1-\frac{1}{\sqrt{x^2+\alpha^2}}\right)\in f\cos\omega\tau-\mu\left[g_1-\alpha\left(1-\frac{1}{\sqrt{x^2+\alpha^2}}\right)\right]\mathrm{Sign}(\dot{x}-v_0), \tag{5}$$

where the dot denotes the differentiation with respect to the dimensionless time τ.

The motion of the mass can be characterized into two qualitatively different modes, the slip and stick modes. During the slip mode, the mass and the belt have different velocities ($\dot{x}\neq v_0$), equation (5) becomes

$$\ddot{x}+c\dot{x}+x\left(1-\frac{1}{\sqrt{x^2+\alpha^2}}\right)=f\cos\omega\tau-\mu\left[g_1-\alpha\left(1-\frac{1}{\sqrt{x^2+\alpha^2}}\right)\right]\mathrm{sign}(\dot{x}-v_0),$$

where $\mathrm{sign}(\cdot)$ is the signum function.

During the stick mode, the mass rests on the belt ($\dot{x}=v_0$), no acceleration exists in this case and equation (5) takes the form

$$\ddot{x}=0.$$

Equation (5) can be rewritten as

$$\ddot{x}=\begin{cases} f\cos\omega\tau - c\dot{x} - x\left(1-\dfrac{1}{\sqrt{x^2+\alpha^2}}\right) \\ -\mu\left[g_1-\alpha\left(1-\dfrac{1}{\sqrt{x^2+\alpha^2}}\right)\right]\mathrm{sign}(\dot{x}-v_0), & \dot{x}\neq v_0, \\ 0, & \dot{x}=v_0, \end{cases} \tag{6}$$

which is called a differential equation with a discontinuous right hand side.[27] A solution of Eq. (6) should be continuously differentiable and piecewise smooth in its domain.

It is worth noting that although the spring itself is linear, this system is strongly nonlinear, having an irrational restoring force[28] $f(x)=x\left(1-1/\sqrt{x^2+\alpha^2}\right)$ due to the geometrical configuration, and a nonconstant friction force $f_{\mathrm{s}}=\mu\left[g_1-\alpha\left(1-1/\sqrt{x^2+\alpha^2}\right)\right]\mathrm{Sign}(\dot{x}-v_0)$, which is relevant to not only the velocity $\dot{x}$, but also the position x.

In the following analysis, we will analyze the equation of motion for the self-excited SD oscillator directly to reflect the natural characters of the system. Furthermore, the friction-induced vibration of multiple stick-slip phenomena and the stick-slip chaos of the perturbed self-excited system will be revealed from the viewpoint of nonlinear dynamics.

3. Equilibrium bifurcation and multiple stick regions

In this section, we discuss the complex phase portraits by investigating the equilibrium and the bifurcation of this system. Let $\dot{x}=y$, equation (3) can be written as

$$\begin{cases} \dot{x}=y, \\ \dot{y}\in -x\left(1-\dfrac{1}{\sqrt{x^2+\alpha^2}}\right) \\ \qquad -\mu\left[g_1-\alpha\left(1-\dfrac{1}{\sqrt{x^2+\alpha^2}}\right)\right]\mathrm{Sign}(y-v_0). \end{cases} \tag{7}$$

It is clear that the equilibrium of system (7) exists when the mass remains still and is continuously slipping on the belt ($y\neq v_0$), then $\mathrm{Sign}(\gamma)=\gamma/|\gamma|$ for $\gamma\neq 0$, and system (7) becomes

$$\begin{cases} \dot{x}=y, \\ \dot{y}=-x\left(1-\dfrac{1}{\sqrt{x^2+\alpha^2}}\right) \\ \qquad -\mu\left[g_1-\alpha\left(1-\dfrac{1}{\sqrt{x^2+\alpha^2}}\right)\right]\mathrm{sign}(y-v_0). \end{cases} \tag{8}$$

Letting $\dot{x}=\dot{y}=0$, the equilibrium of system (8) can be obtained by solving the following equation:

$$x\left(1-\frac{1}{\sqrt{x^2+\alpha^2}}\right)-\mu\left[g_1-\alpha\left(1-\frac{1}{\sqrt{x^2+\alpha^2}}\right)\right]=0. \tag{9}$$

By using transposition and square, equation (9) can be rewritten as

$$x^4+2\mu(\alpha-g_1)x^3+[\alpha^2-1+\mu^2(\alpha-g_1)^2]x^2 +2\mu\alpha(\alpha^2-g_1\alpha-1)x+\mu^2\alpha^2[(\alpha-g_1)^2-1]=0. \tag{10}$$

By employing the method for solving quartic equations,[29] the solutions to Eq. (10) are obtained as

$$\begin{aligned} x_1&=\frac{1}{2}\mu(g_1-\alpha)-\frac{1}{2}\sqrt{\Upsilon_1+\Delta}+\frac{1}{2}\sqrt{2\Upsilon_1-\Delta-\Upsilon_2}, \\ x_2&=\frac{1}{2}\mu(g_1-\alpha)-\frac{1}{2}\sqrt{\Upsilon_1+\Delta}-\frac{1}{2}\sqrt{2\Upsilon_1-\Delta-\Upsilon_2}, \\ x_3&=\frac{1}{2}\mu(g_1-\alpha)+\frac{1}{2}\sqrt{\Upsilon_1+\Delta}+\frac{1}{2}\sqrt{2\Upsilon_1-\Delta+\Upsilon_2}, \\ x_4&=\frac{1}{2}\mu(g_1-\alpha)+\frac{1}{2}\sqrt{\Upsilon_1+\Delta}-\frac{1}{2}\sqrt{2\Upsilon_1-\Delta+\Upsilon_2}, \end{aligned} \tag{11}$$

where

$$\begin{aligned} \Upsilon_1 &= \frac{1}{3}(\mu\alpha-\mu g_1)^2-\frac{2}{3}(\alpha^2-1), \\ \Upsilon_2 &= \{8(\mu g_1-\mu\alpha)^3-16\mu\alpha(\alpha^2-g_1\alpha-1)+8(\mu\alpha-\mu g_1) \\ &\quad\times[(\mu\alpha-\mu g_1)^2+\alpha^2-1]\}/(4\sqrt{\Upsilon_1+\Delta}), \\ \Delta &= \frac{\sqrt[3]{2}\Delta_1}{3\sqrt[3]{\Delta_2+\sqrt{-4\Delta_1^3+\Delta_2^2}}}+\frac{\sqrt[3]{\Delta_2+\sqrt{-4\Delta_1^3+\Delta_2^2}}}{3\sqrt[3]{2}}, \\ \Delta_1 &= 12\mu^2\alpha^2[(g_1-\alpha)^2-1]-12(\mu\alpha-\mu g_1) \\ &\quad\times(\mu\alpha^3-\mu\alpha^2 g_1-\mu\alpha)+[(\mu\alpha-\mu g_1)^2+\alpha^2-1]^2, \\ \Delta_2 &= 108\mu^2\alpha^2(\mu\alpha-\mu g_1)^2[(\alpha-g_1)^2-1] \\ &\quad-72\mu^2\alpha^2[(\alpha-g_1)^2-1][(\mu\alpha-\mu g_1)^2+\alpha^2-1] \\ &\quad-36(\mu\alpha-\mu g_1)(\mu\alpha^3-\mu\alpha^2 g_1-\mu\alpha) \\ &\quad\times[(\mu\alpha-\mu g_1)^2+\alpha^2-1]+108(\mu\alpha^3-\mu\alpha^2 g_1-\mu\alpha) \\ &\quad+2[(\mu\alpha-\mu g_1)^2+\alpha^2-1]^3. \end{aligned}$$

However, x_4 is not the solution of Eq. (9), since

$$x_4\left(1-\frac{1}{\sqrt{x_4^2+\alpha^2}}\right)-\mu\left[g_1-\alpha\left(1-\frac{1}{\sqrt{x_4^2+\alpha^2}}\right)\right]\neq 0. \tag{12}$$

Therefore, the equilibria of system (3) are a saddle point $(x_1,0)$ and two centers $(x_2,0)$ and $(x_3,0)$ [see Fig. 3(b)]. The equilibrium surface in (x,α,μ) space is shown in Fig. 2(a), from which we see clearly the equilibria bifurcation of the self-excited system for the variation of parameters α and μ.

For a better overview, the variation of one parameter while the other one is kept constant is shown in two section planes: β_1 shows the variation of α for a constant μ [Fig. 2(b)] and β_2 shows the variation of μ for a constant α [Fig. 2(c)], in which the solid and dashed curves represent the stable and unstable branches, respectively.

The transition sets $\mathcal{H}$ in the parameter space (μ,α) are obtained and plotted in Fig. 3(M), where

$$\mathcal{H} = \{(\alpha,\mu)|2\Upsilon_1(\alpha,\mu)-\Delta(\alpha,\mu)-\Upsilon_2(\alpha,\mu)=0,$$

$\alpha, \mu > 0\}$. (13)

Obviously, the equilibria of system (3) depend on parameters α and μ as shown in Fig. 2(a). In order to examine the influence of parameters α and μ on the dynamics of system (3), the bifurcation diagram is constructed and depicted in Fig. 3(M). In the parameter space (α, μ), the surface can be divided into two persistence regions marked by I and II with $\mathcal{H}$, as shown in Fig. 3. Suppose that a point $Q(\alpha, \mu)$ in the parameter plane (α, μ) starts from region II and enters region I, the stationary $(x_1, 0)$ state exhibits the transition from hyperbolic structure to non-hyperbolic at $\mathcal{H}$, and the system undergoes a center-saddle bifurcation [depicted in Figs. 2(b) and 2(c)] at $\mathcal{H}$, where the equilibria change from three equilibria (a saddle $(x_1, 0)$ and two centers $(x_2, 0)$, $(x_3, 0)$) to two (a non-hyperbolic equilibrium $(x_1, 0)$ and a center $(x_3, 0)$), and finally into one (a center $(x_3, 0)$). Furthermore, the system also undergoes a double tangency bifurcation[30] at $\mathcal{H}$ where the three stick regions of the system merge into one large stick region from region II to region I.

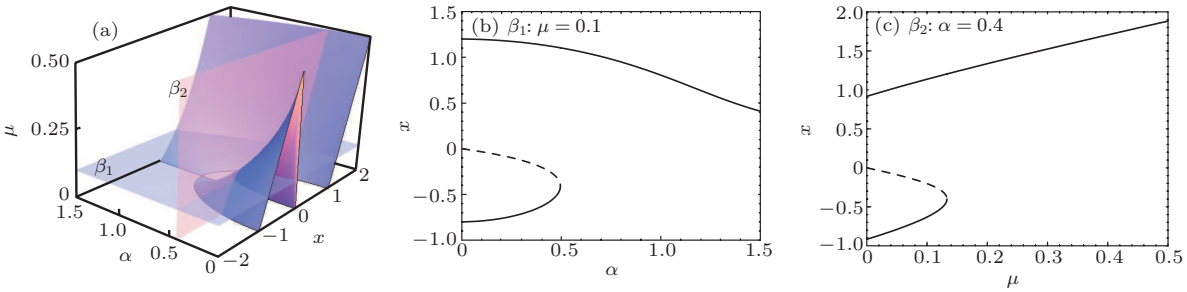


Fig. 2. (color online) Equilibrium surface in (x, α, μ) space and sections β_1 and β_2 (the solid and dashed curves represent the stable and unstable branches, respectively). (a) Equilibrium surface. Panels (b) and (c) show center-saddle bifurcation in x–α plane (section β_1) for $\mu = 0.1$ and in x–μ plane (section β_2) for $\alpha = 0.4$, respectively.

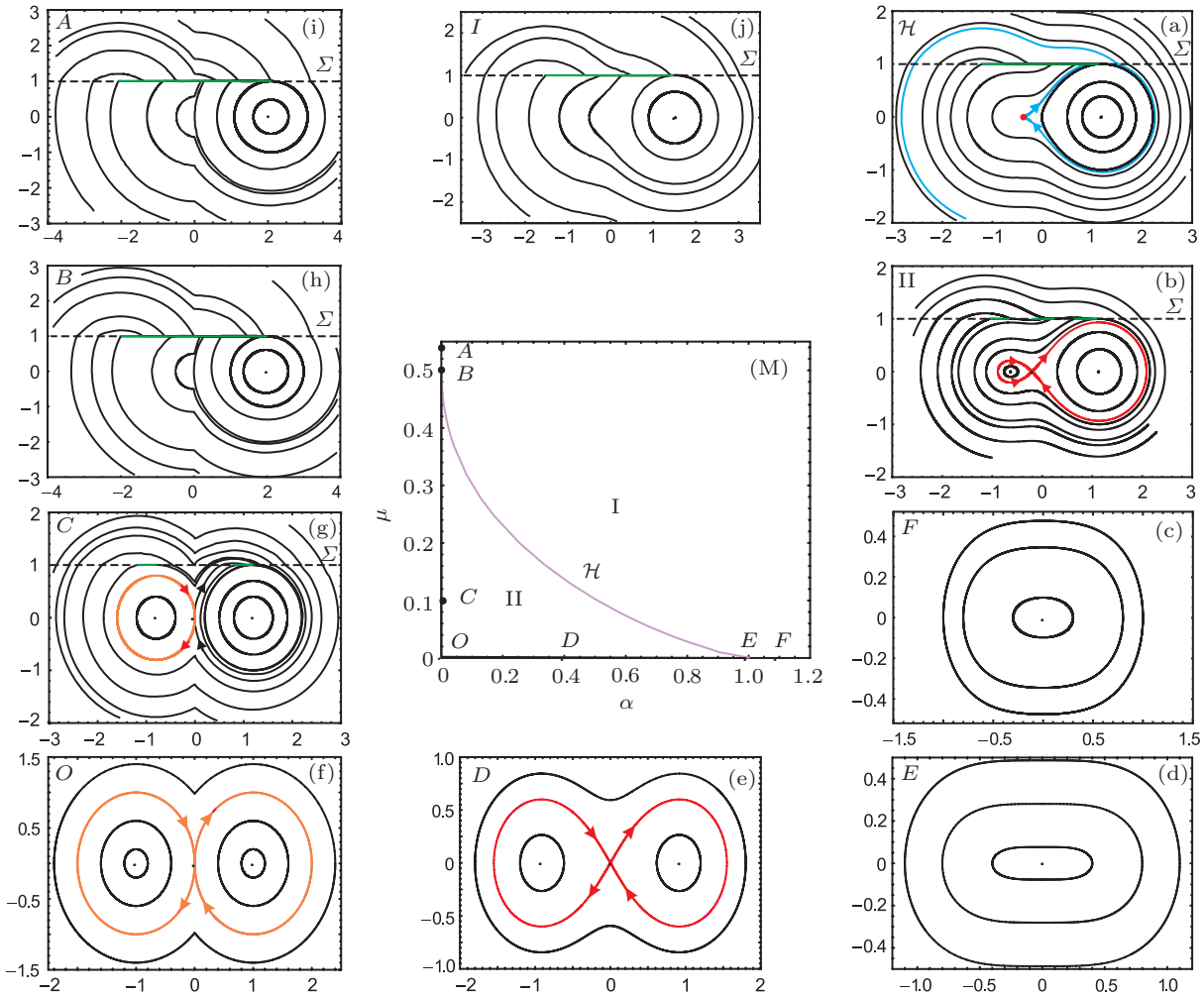


Fig. 3. (color online) (M) Bifurcation diagram and the corresponding phase portraits of different symbols. The $\mathcal{H}$ transition sets divide parameter space (α, μ) into two persistent regions marked by I and II and the corresponding phase portraits of system (3) are presented in panels (a)–(j).

All the corresponding phase portraits of system (3) are presented in Figs. 3(a)–3(j), the corresponding symbols are marked in Fig. 3(M). The blue and red dots denote the centers and the saddle points connecting the corresponding homoclinic orbits, respectively, see Figs. 3(b) and 3(e). Meanwhile small cycles indicate non-standard or saddle-like equilibria[23,25] connecting the corresponding homoclinic-like orbits, as shown in Figs. 3(f) and 3(g). In particular, figure 3(a) shows an orbit (marked by blue) connecting with a non-hyperbolic equilibrium called the center-saddle point (with double eigenvalues 0). In all the phase portraits of system (3) shown in Figs. 3(a)–3(j), the symbol Σ denotes the discontinuous boundary $y = 1$ for this self-excited system, and the stick regions marked by green indicate that the mass has the same velocity with the belt.

Hence, the difference between the SD oscillator and the self-excited SD oscillator can be seen from Fig. 3. For $\mu = 0$, system (3) becomes the SD oscillator shown in Figs. 3(c)–3(f). For $\mu \neq 0$, figures 3(a), 3(b), 3(g), and 3(j) present the phase portraits of the self-excited SD oscillator. Obviously, the moving belt friction destroys the symmetry of the original SD oscillator. In conclusion, the self-excited SD oscillator with dry friction is characterized by a friction-induced asymmetry and multiple stick regions in the phase plane.

4. The perturbed dynamics

An overview of the dynamical and bifurcation behavior of the self-excited SD oscillator with simultaneous viscous damping and external harmonic excitation will be given in this section. Numerical simulations are carried out to further investigate the belt friction-induced nonlinear dynamics and to explore the multiple stick-slip patterns of the perturbed self-excited system.

4.1. The effect of damping and belt velocity

In this subsection, the dynamic behavior of the self-excited SD oscillator with a linear damping is investigated. For the case of $c \neq 0$ and $f = 0$, system (5) takes the form

$$\ddot{x} + c\dot{x} + x\left(1 - \frac{1}{\sqrt{x^2+\alpha^2}}\right) \in -\mu\left[g_1 - \alpha\left(1 - \frac{1}{\sqrt{x^2+\alpha^2}}\right)\right]\mathrm{Sign}(\dot{x} - v_0). \quad (14)$$

The equilibria of this damped self-excited system are the same as those of system (7). The equilibria $(x_2, 0)$ and $(x_3, 0)$ of the system are stable, marked by yellow dots in Fig. 4, and the basins of attraction of the equilibria are also plotted. The equilibrium $(x_1, 0)$ denoted by a black dot still has the property of the saddle point $(\alpha = 0.4)$ and the saddle-like point $(\alpha = 0)$ as that of system (7), which is located in the basin boundary. This boundary is the stable manifold of the equilibrium $(x_1, 0)$. It is the separatrix curve which separates the basins of attraction of equilibria $(x_2, 0)$ and $(x_3, 0)$. In Figs. 4(a)–4(d), the dynamic behavior of friction-induced asymmetry for this self-excited system is presented, furthermore, this asymmetry becomes more obvious when the belt velocity v_0 increases. For $\mu = 0$, system (14) becomes the SD oscillator which has no friction, and its basins of attraction are symmetrical, as shown in Figs. 4(e) and 4(f).

4.2. Bifurcation behaviors and coexisting attractors

In this subsection, we investigate the dynamic behavior of system (5) affected by the external excitation from the nonlinear dynamics point of view. It is found that there coexists period doubling leading to the coexistence of chaotic attractor

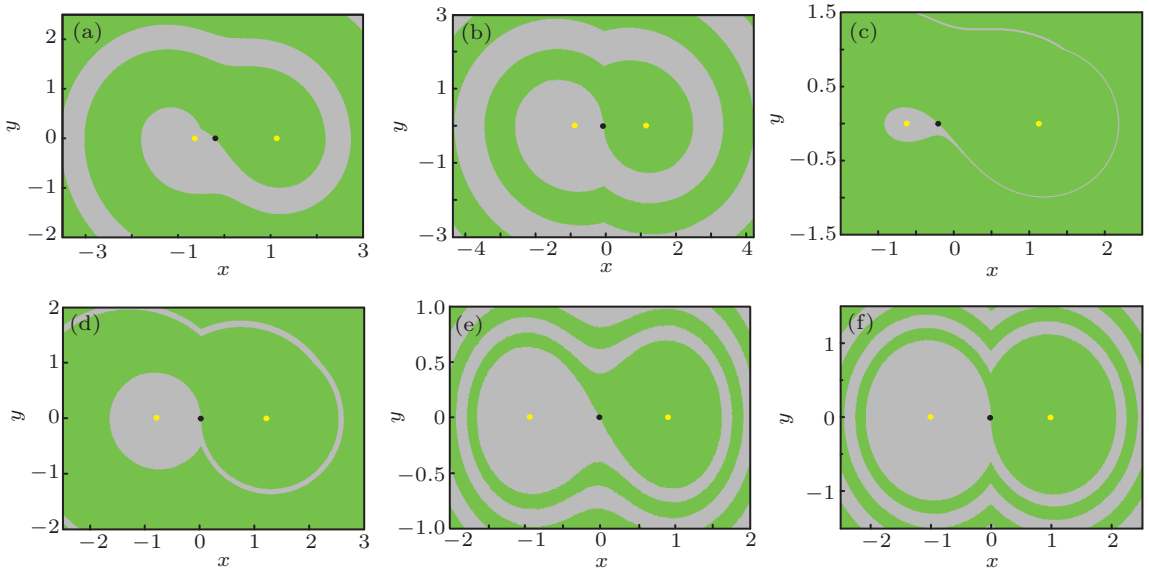


Fig. 4. (color online) Basin analysis of system (14) for $c = 0.048$. The basins of attraction are shown in grey for equilibrium $(x_2, 0)$ and in green for equilibrium $(x_3, 0)$. The yellow dots denote points $(x_2, 0)$ and $(x_3, 0)$, while the black dots indicate equilibrium $(x_1, 0)$. (a) $\alpha = 0.4$ and (b) $\alpha = 0$ for belt velocity $v_0 = 0.2$. (c) $\alpha = 0.4$ and (d) $\alpha = 0$ for belt velocity $v_0 = 1$. (e) $\alpha = 0.4$ and (f) $\alpha = 0$ for system (14) with no friction ($\mu = 0$).

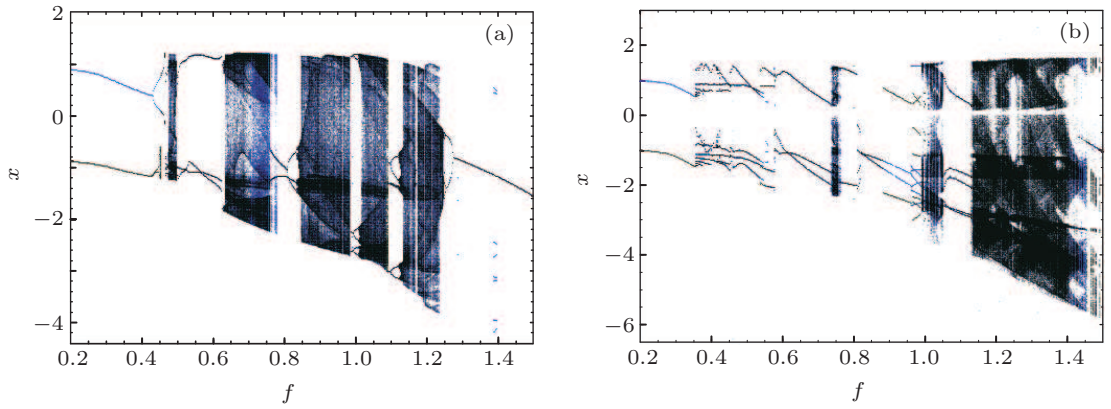


Fig. 5. (color online) Bifurcation diagrams of two coexisting attractors (blue and black) for displacement x versus f, where $v_0 = 0.2$; (a) $\alpha = 0.4$, and (b) $\alpha = 0$.

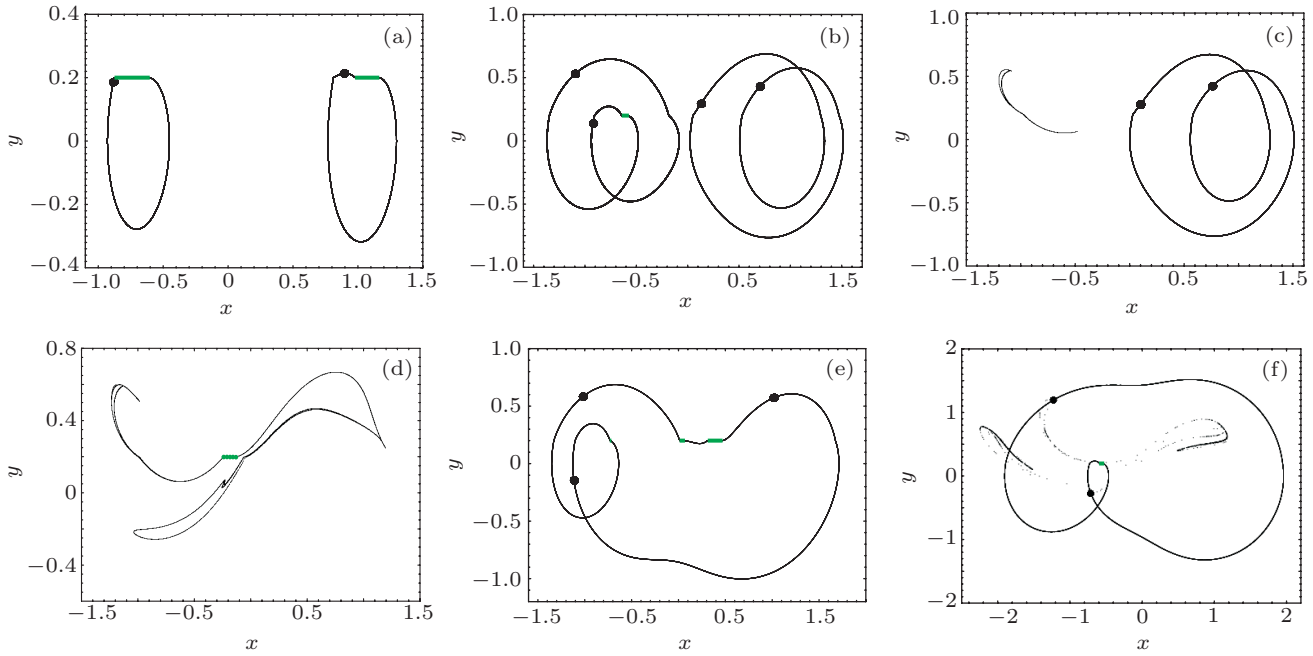


Fig. 6. (color online) Periodic motions and chaotic attractors of system (5) for $\alpha = 0.4$. (a) Coexisting stick-slip period-1 solutions for $f = 0.2$. (b) Coexisting period-2 solutions for $f = 0.449$. (c) Coexistence of a period-2 solution and a chaotic attractor for $f = 0.453$ with the largest Lyapunov exponent 0.0475. (d) Chaotic attractor for $f = 0.48$ with the largest Lyapunov exponent 0.0563. (e) Period-3 solution with three stick-slip motions for $f = 0.51$. (f) Coexistence of a stick-slip period-2 solution and a chaotic attractor for $f = 0.7645$ with the largest Lyapunov exponent 0.0538.

and period solution, or merging to a large chaotic motion[31–33] as the parameter varies.

The bifurcation diagrams for the displacement x versus the harmonic excitation force f have been constructed as f increases from 0.2 to 1.5 for two different initial conditions $(x_0, y_0) = (1, 0)$ (blue) and $(x_0, y_0) = (-1, 0)$ (black), as shown in Fig. 5(a) for $\alpha = 0.4$ and Fig. 5(b) for $\alpha = 0$, assuming $c = 0.048$, $g_1 = 2$, $\mu = 0.1$, $v_0 = 0.2$, and $\omega = 1.08$. From Figs. 5(a) and 5(b), the existence of a pair of period doubling series can be seen in the bifurcation diagrams.

In all of the following phase portraits, the cusps correspond to a sign change of the relative velocity, and the short horizontal parts (marked with green lines) in the phase portraits correspond to sticking during the motion.

Case I When $\alpha = 0.4$, these two coexisting stick-slip period-1 solutions are asymmetric, the orbits of motion for $f = 0.2$ are shown in Fig. 6(a). The sticking of these motions exists in two different stick regions. The slip trajectory is always below the stick trajectory on the left side. On the right side, the trajectory consists of a stick phase, plus a slip phase above the stick trajectory ($y > v_0$) and a slip phase below the stick trajectory ($y < v_0$), and the motion is also called a slip-stick-slip motion.

With the increase of excitation amplitude f, a coexisting pair of asymmetric period doubling can be observed in Fig. 5(a), a pair of asymmetric coexisting period-2 solutions are presented in Fig. 6(b) for $f = 0.449$, where one is a solution of stick-sip motion and the other is a solution of pure slip motion. When $f = 0.453$, a chaotic attractor coexists with a period-2 solution of pure slip motion, and the corresponding trajectories and the chaotic attractor are shown in Fig. 6(c). With the increase of f, these solutions can merge into a single

stick-slip chaotic attractor, which is a peculiar character of the friction system, as presented in Fig. 6(d) when f increases to $f = 0.48$, and finally merge into a stick-slip period-3 solution, as shown in Fig. 6(e) when $f = 0.51$. The coexistence of a chaotic attractor and a stick-slip period-2 solution are shown in Fig. 6(f) when $f = 0.7645$.

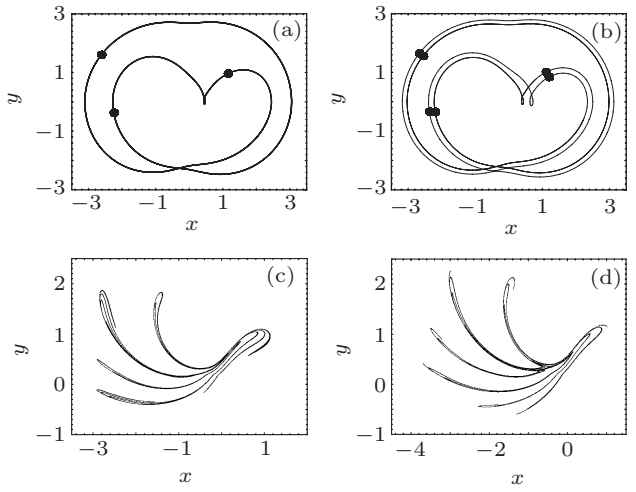


Fig. 7. Period-3 doubling and chaotic attractors for $\alpha = 0.4$. (a) Period-3 solution for $f = 0.9868$. (b) Period-6 solution for $f = 1$. (c) and (d) Chaotic attractors for $f = 1.07$ and $f = 1.2$ with the largest Lyapunov exponents 0.0805 and 0.0781, respectively.

Similarly, as f further increases, the process of a period-3 doubling leading to chaos can be observed from Fig. 5(a), as well as from the period-3 solution shown in Fig. 7(a) for $f = 0.9868$, bifurcating to period-6 solution in Fig. 7(b) for $f = 1$, to the chaotic attractors in Fig. 7(c) for $f = 1.07$ and Fig. 7(d) for $f = 1.2$.

It is most interesting that the stick-slip period-3 motion depicted in Fig. 6(e) contains three stick phases, which demonstrates the friction induced vibration of multiple stick-slip phenomena for the perturbed self-excited system. As an interesting detail, we can see that for large amplitudes f of the excitation, shortening [Figs. 6(b) and 6(e)] or disappearance [Figs. 7(a) and 7(b)] of the stick mode becomes possible. Pushed by the spring force and the external excitation, the mass overtakes the belt or slows down re-entering the stick mode after a small wiggle, as shown in Fig. 6(e).

Case II When $\alpha = 0$, there exist a pair of asymmetric stick-slip period-1 solutions for $f = 0.2$, as shown in Fig. 8(a), where these motions of sticking are in two stick regions. With the increase of f, these motions can merge into a single period-8 solution with three stick-slip motions as shown in Fig. 8(b) for $f = 0.38$, which also presents the friction-induced vibration of multiple stick-slip phenomena for the perturbed self-excited system. A single period-3 solution without sticking is shown in Fig. 8(c) when f increases to $f = 0.7$, and a chaotic attractor is presented in Fig. 8(d) when $f = 0.75$.

With the increase of f, the coexisting period-2 solutions without sticking shown in Fig. 9(a) for $f = 0.95$ bifurcate to a pair of period-7 solutions without sticking in Fig. 9(b) for $f = 0.975$, and finally merge into a chaotic attractor in Fig. 9(c) for $f = 1.02$ and a chaotic attractor in Fig. 9(d) for $f = 1.34$.

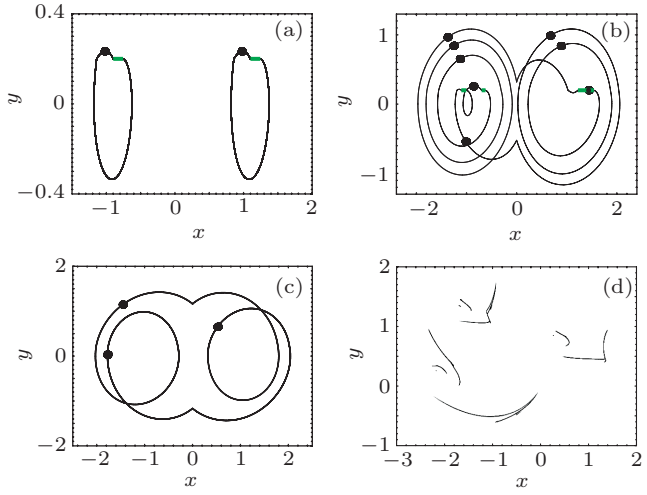


Fig. 8. (color online) Periodic motions and chaotic attractor of system (5) for $\alpha = 0$. (a) Coexisting stick-slip period-1 solutions for $f = 0.2$. (b) Period-8 solution for $f = 0.38$. (c) Period-3 solution for $f = 0.7$. (d) Chaotic attractor for $f = 0.75$ with the largest Lyapunov exponent 0.0218.

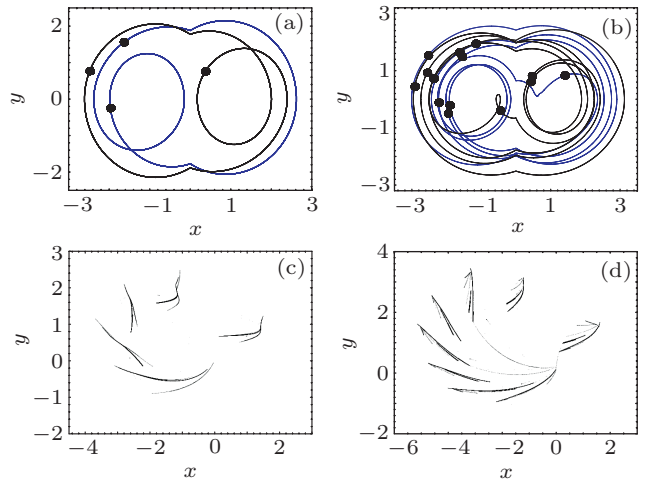


Fig. 9. (color online) Coexistence of periodic motions and chaotic attractors of system (5) for $\alpha = 0$. (a) Coexisting period-2 solutions for $f = 0.95$. (b) Coexisting period-7 solutions for $f = 0.975$. (c) Chaotic attractor for $f = 1.02$ with the largest Lyapunov exponent 0.0159. (d) Chaotic attractor for $f = 1.34$ with the largest Lyapunov exponent 0.018.

4.3. Basin analysis of coexisting attractors

Basin analysis is carried out for investigating the complex coexistence of multiple attractors in system (5) by using Poincaré sections, as shown in Figs. 10(a)–10(d) for $c = 0.048$, $g_1 = 2$, $\mu = 0.1$, $v_0 = 0.2$, $\omega = 1.08$ and different values of α and f. When $\alpha = 0.4$, the basins (marked green and grey) of a pair of period 1 solutions (yellow and black) are shown for $f = 0.3$ in Fig. 10(a). If increasing f to 0.4528, there coexist a chaotic attractor (black) and a period-2 solution (yellow), as presented in Fig. 10(b), and their basins are colored grey and green, respectively.

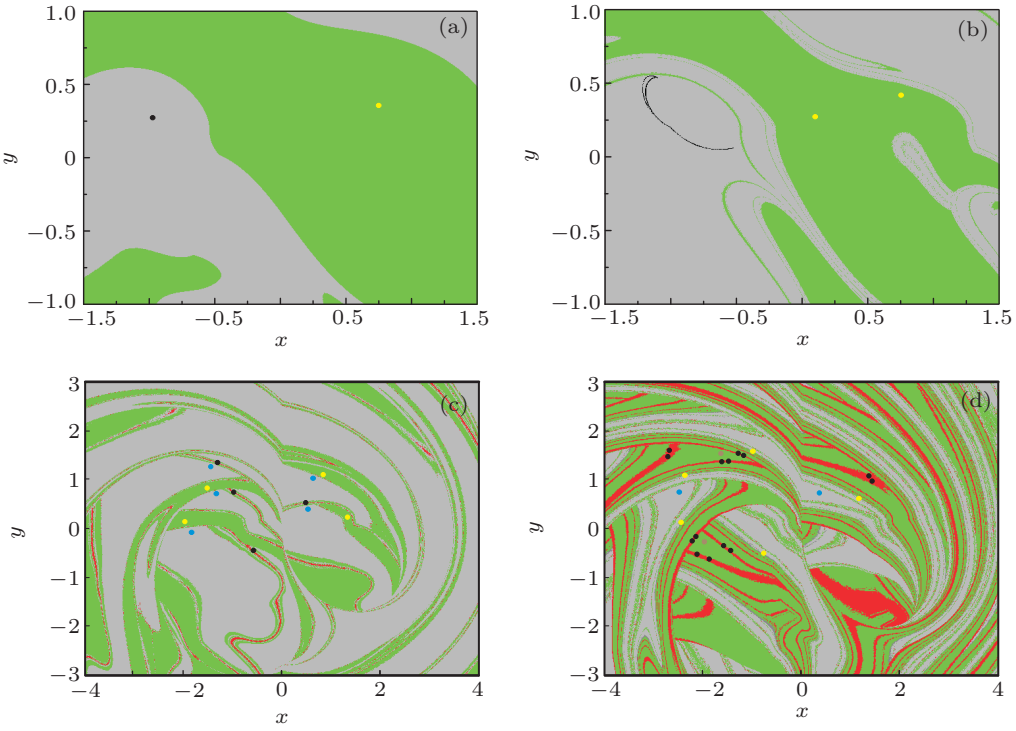


Fig. 10. (color online) Basins of attraction and their corresponding coexisting attractors using Poincaré sections for $c = 0.048$, $g_1 = 2$, $\mu = 0.1$, $v_0 = 0.2$, and $\omega = 1.08$. (a) Coexisting period-1 solutions (black and yellow) for $\alpha = 0.4$ and $f = 0.3$. (b) Coexistence of a period-2 solution (yellow) and a chaotic attractor (black) for $\alpha = 0.4$ and $f = 0.4528$ with the largest Lyapunov exponent 0.0482. (c) Coexistence of a pair of period-4 solutions (black and yellow) and a period-5 solution (blue) for $\alpha = 0$ and $f = 0.54$. (d) Coexistence of a pair of period-2 solutions (brown and blue), a period-5 solution (yellow), and a period-14 solution (black) for $\alpha = 0$ and $f = 0.95$.

System (5) has not just one or two-coexisting attractors, but probably multiple coexisting attractors in some cases. Figure 10(c) shows the basins (marked green, red, and grey) of a pair of period-4 solutions (yellow and black) and a period-5 solution (blue) for $\alpha = 0$ and $f = 0.54$. When f increases to 0.95, as shown in Fig. 10(d), there are the basins (green, grey, dark grey, and red) of a pair of period-2 solutions (brown and blue), a period-5 solution (yellow), and a period-14 solution (black).

The largest Lyapunov exponents for all the chaotic attractors presented in this non-smooth system have been obtained by employing the chaos synchronization method,[34] as shown in the captions of the figures.

5. Conclusion

In this paper, we have proposed a novel self-excited SD oscillator driven by moving belt friction. The mathematical model of the belt-driven system has been investigated, where the friction characteristic is modeled as the Coulomb friction. The equilibrium states and bifurcation structures have been investigated. The self-excited system is characterized by the existence of multiple stick regions in the phase portraits which exhibit the hyperbolic structure transition and friction-induced asymmetry phenomena. Under perturbation, the system exhibits complex coexistence of periodic attractors and also the periodic solution with a chaotic attractor, which presents the friction-induced vibration of multiple stick-slip phenomena and the stick-slip chaos in the self-excited system in the presence of viscous damping and an external harmonic force.

The presented oscillator is being actively studied by the authors in two main directions. Firstly, the peculiar properties of multiple stick regions, the hyperbolic structure transition, and the friction-induced asymmetry of this oscillator are being analyzed to better understand the belt friction-induced nonlinear dynamics. The second pursued direction is to focus on the experimental research to measure the related friction characteristic for this belt-driven oscillator. We are currently working in these directions.

References

[1] Rhee S K, Tsang P H S and Wang Y S 1989 *Wear* **133** 39
[2] Cao Q J, Friswell M I, Ouyang H, Mottershead J E and James S 2003 *Mater. Scien. Foru.* **440** 269
[3] Ouyang H, Cao Q J, Mottershead J E and Treyde 2003 *Proceedings of the Institution of Mechanical Engineers Part D: Journal of Automobile Engineering* **271** 867
[4] Madoliat R, Hayati S and Ghalebahman A G 2011 *Scient. Irani.* **18** 1069
[5] Wiercigroch M and Krivtsov A 2001 *Phil. Trans. R. Soc. Lond. A* **359** 713
[6] Mihajlović N, Van Veggel A A, Van de Wouw N and Nijmeijer H 2004 *J. Dyn. Sys. Meas. Control* **126** 709
[7] Mihajlović N, Van de Wouw N, Hendriks M P M and Nijmeijer H 2006 *Non. Dyn.* **46** 273
[8] Luo A C J and Gegg B C 2006 *J. Sound Vibr.* **291** 132
[9] Li Q H, Chen Y M and Qin Z Y 2011 *Chin. Phys. Lett.* **28** 030502
[10] Sándor B, Járai-Szabó F, Tél T and Néda Z 2013 *Phys. Rev. E* **87** 042920
[11] You H I and Hsia J H 1995 *J. Tribology ASME* **117** 450

[12] Abdo J and Abouelsoud A A 2011 *J. Theoretic. Appl. Mecha.* **49** 971
[13] Hetzler H, Schwarzer D and Seemann W 2007 *Commun. Nonlin. Sci.* **12** 83
[14] Narayanan S and Jayaraman K 1991 *J. Sound Vibr.* **146** 17
[15] Luo A C J and Huang J Z 2012 *Nonlin. Anal. Real World Appli.* **13** 241
[16] Li Q H, Yan Y L, Wei L M and Qin Z Y 2013 *Acta Phys. Sin.* **62** 120505 (in Chinese)
[17] Ouyang H and Mottershead J E 1998 *J. Sound Vibr.* **209** 251
[18] Mohammed A A Y and Rahim I A 2013 *I. J. Scien. Tech. Research* **2** 60
[19] Li B 2007 *Analysis of Non-smooth Dynamics of Brake System with Dry-Friction* (MS Thesis) (Tianjin: Tianjin University) (in Chinese)
[20] Burridge R and Knopoff L 1967 *Bull. Seismol. Soc. Am.* **57** 341
[21] Carlson J M and Langer J S 1989 *Phys. Rev. A* **40** 6470
[22] Sergienko O V, Macayeal D R and Bindschadler R A 2009 *Annals of Glaciology* **50** 87
[23] Thompson J M T and Hunt G W 1973 *A general theory of elastic stability* (London: Wiley)
[24] Cao Q J, Wiercigroch M, Pavlovskaia E E, Grebogi C and Thompson J M T 2006 *Phys. Rev. E* **74** 046218
[25] Cao Q J, Wiercigroch M, Pavlovskaia E E, Thompson J M T and Grebogi C 2008 *Phil. Trans. R. Soc. A* **366** 635
[26] Cao Q J, Wiercigroch M, Pavlovskaia E E, Grebogi C and Thompson J M T 2008 *Int. J. Nonlin. Mech.* **43** 462
[27] Filippov A F 1988 *Differential Equations with Discontinuous Right-hand Sides* (Dordrecht: Kluwer Acadamic)
[28] Tian R L, Yang X W, Cao Q J and Wu Q L 2012 *Chin. Phys. B* **21** 050503
[29] Fathi A and Sharifan N 2013 *Appl. Comput. Math.* **2** 24
[30] Kuznetsov Y A, Rinaldi S and Gragnani A 2003 *Int. J. Bifur. Chaos* **13** 2157
[31] Jiang G R, Xu B G and Yang Q G 2009 *Chin. Phys. B* **18** 5235
[32] Zhang Y and Bi Q S 2011 *Chin. Phys. B* **20** 010504
[33] Jiang H B, Zhang L P and Yu J J 2015 *Chin. Phys. B* **24** 020502
[34] Stefanski A and Kapitaniak T 2000 *Disc. Dyn. Nat. Soc.* **4** 207